ISSN 1392-1207. MECHANIKA. Vol. 31, No. 6, 2025: 531–540

Numerical Simulation of a Binary Fluid Behavior Subjected to the Coupling Between Natural Convection and Thermodiffusion in a Partially Wavy Cavity

Mohamed Abdelhak MAAZOUZI*, Ali BENZEGAOU, Nazihe TARFAYA*****

**Mechanics Laboratory, Modeling and Experiments (L2ME), Department of Mechanical Engineering, University Tahri Mohammed, Bechar, Algeria, 08000, E-mail: maazouzi.mohamed@univ-bechar.dz (Corresponding Author)*

***Mechanics Laboratory, Modeling and Experiments (L2ME), Department of Mechanical Engineering, University Tahri Mohammed, Bechar, Algeria, 08000, E-mail: benzegaou.ali@univ-bechar.dz*

***FIMAS Laboratory, Department of Mechanical Engineering, University Tahri Mohammed, Bechar, Algeria, 08000, E-mail: Terfaya.nazihe@univ-bechar.dz*

https://doi.org/10.5755/j02.mech.42356

Nomenclature

A - aspect ratio (shape factor); $\hat{a}$ - amplitude of the undulations, m; a - dimensionless amplitude of the undulations; $\hat{c}$ - mass fraction of the component considered; $\hat{C}$ - mass concentration, Kg/m^3; C - dimensionless mass concentration; D - mass diffusion coefficient, m^2/s; D_T - thermodiffusion coefficient, m^2/sK; g - gravitational acceleration, m/s^2, H - cavity height, m; L - cavity width, m; L_w - dimensionless length of the undulated section; Le - Lewis number; N - dimensionless normal coordinate; n - normal coordinate, m; P - dimensionless pression; Pr - Prandtl number; Ra - thermal Rayleigh number; t - dimensionless time; $\hat{T}$ - dimensional local temperature, K; T - dimensionless local temperature; T_b, T_h - dimensionless temperatures at the bottom and top of the cavity; $V(U, V)$ - dimensionless velocity vector; x, z - horizontal and vertical dimensionless coordinates.

Greek symbols

ρ - density, kg/m^3; μ - dynamic viscosity, Pa.s; v - kinematic viscosity, m^2/s; α - thermal diffusivity, m^2/s; Ψ - separation ratio; β_T - thermal expansion coefficient, 1/K; β_C - solutal expansion coefficient.

1. Introduction

The homogeneity of a multi-component mixture, such as a binary mixture is destroyed by the influence of a temperature gradient. This thermal gradient induces an additional mass diffusion, resulting in a concentration gradient. This physical phenomenon, discovered in the 19th century by Ludwig (1856) and later by Soret (1879), is known as “thermodiffusion”, or the “Ludwig-Soret effect”, more commonly referred to as the “Soret effect”. It involves the separation of a component’s mixture towards regions of varying temperature within a domain that exhibits a non-uniform temperature distribution.

In addition to Fick's classical law, the temperature gradient in binary fluid mixtures causes a material displacement effect. The total mass flux J_m includes the contribution from the concentration gradient as well as from the temperature gradient [1]:

$$\vec{J}_m = -\rho D \nabla \hat{c} - \rho \hat{c}\left(1-\hat{c}\right) D_T \nabla \hat{T}. \quad (1)$$

In other words, $\nabla \hat{c}$ is the mass fraction gradient induced by the temperature gradient $\nabla \hat{T}$, D is the mass diffusion coefficient, D_T is the thermodiffusion coefficient, ρ is the density, and $\hat{c}$ is the mass fraction of the component considered.
When this phenomenon, interacts with convection, it leads to "thermogravitational diffusion." This resulting phenomenon, in a binary fluid, refers to the movement of species in a mixture under the combined effect of a temperature gradient and gravity. It occurs in many practical applications, such as separation and purification of liquid or gas mixtures, stratification of fluids in natural or oceanic reservoirs, isotopic refinement, crystallization and crystal formation, and the manufacture of composite materials and alloys. Under certain thermal, dynamic, and geometric conditions, this interaction can amplify the separation of species.

The study of thermogravitational separation has undergone remarkable evolution since the pioneering work of Clusius and Dickel [2], who demonstrated, using the thermogravitational column (TGC), that a gas mixture confined between two concentric cylinders, with the inner cylinder heated and the other cooled, exhibits a variation in gas concentration between the bottom and the top of the column. In 1939, the first theoretical interpretation of this phenomenon was proposed by Furry, Jones, and Onsager (FJO) [3], who developed a fundamental model for isotopic separation in the Clusius-Dickel column. The authors did not take into account the influence of the concentration gradient on the density gradient in the buoyancy force term (an overlooked effect). In 1942, the (FJO) theory was extended to liquids by De Groot [4], thereby laying the phenomenological foundations of thermogravitational separation in fluids.

Subsequently, other authors suggested improvements to experimental systems to increase the efficiency of mixture separation. Their suggestions involved varying the geometry of the separation systems and their position in the gravitational field, as well as varying the boundary conditions and the medium containing the mixture. Lorenz and Emery [5] introduced a porous medium into the column (TGC) to enhance mass transfer, while Platten, Bou-Ali, and Dutrieux [6] showed that tilting the cavity relative to the vertical could significantly accelerate molecular separation. Unlike vertical thermo-gravitational columns, Elhajjar et al. [7] proposed a new method to improve the separation rate of species in a binary fluid mixture. They used a cavity

heated horizontally at the top, subjected to a uniform horizontal temperature gradient along the horizontal walls. Charrier-Mojtabi, Elhajjar, and Mojtabi [8] developed a linear stability analysis of the single-cell flow, which occurs at the onset of convection of a binary fluid in a horizontal porous cavity heated from below. Another study conducted by Elhajjar, Mojtabi, and Charrier-Mojtabi [9] examined the impact of high-frequency, low-amplitude vertical vibrational excitations on the stability of single-phase flow in a shallow horizontal porous layer saturated with a binary fluid and heated from below. Subsequently, Elhajjar et al. [10] theoretically and numerically studied species separation in an inclined porous cavity.

In another geometric and physical configuration, Khouzam et al. [11] studied the separation of species in a binary fluid mixture. The binary mixture is confined in a horizontal rectangular cavity, heated either from the top or the bottom, at different uniform temperatures on its impermeable horizontal walls. The upper horizontal wall moves at a uniform speed. The separation as a function of the Péclet number and the Rayleigh number was determined analytically and numerically. Further studies were conducted on porous layers saturated with a binary fluid, with different boundary conditions. Mojtabi et al. [12] considered a new configuration to separate the components of a binary mixture saturating a horizontal porous layer in a cavity with moving walls. Then, a numerical and analytical study was carried out by Mojtabi et al. [13] for species separation in an horizontal annular porous column. On the other hand, Sioud et al. [14] conducted a comparative study on thermogravitational separation in vertical and horizontal porous annular cylindrical cells saturated with a binary water-ethanol mixture.

More recently, Mojtabi, Sioud, and Charrier-Mojtabi [15] proposed an innovative approach for continuous separation of species in an open porous thermogravitational column, combining natural and forced convection. These authors demonstrated that, for the same temperature difference, the porous medium allows a separation rate up to twenty times higher than that obtained in a conventional fluid device, thus paving the way for larger-scale applications.

Resent research aims to better quantify the actual coupling between temperature, concentration, and density gradients, to identify optimal geometric configurations (inclination, vibration, porosity, wall mobility) that improve separation efficiency, and to design continuous or hybrid thermogravitational systems suitable for larger-scale applications

This current work proposes a numerical study of the hydrodynamic, mass, and thermal behavior of a binary fluid in a new geometric configuration. The fluid is confined in a modified horizontal rectangular enclosure, heated either from the bottom or from the top, featuring partial undulations on its horizontal walls, which are impermeable and isothermal at respective temperatures $\hat{T}_b$ (at the bottom) and $\hat{T}_h$ (at the top). The vertical walls are considered perfectly insulated. The objective of this study is to analyze the separation of the fluid species based on its behavior under the effect of the imposed geometric and thermal constraints.
The physical model and mathematical formulation of the problem are presented in section two, followed by the numerical results in section three and conclusions in section four.

2. Physical Model and Mathematical Formulation

2.1. Physical model

Fig. 1 illustrates the studied physical configuration, a rectangular enclosure featuring partial undulations on both its top and bottom horizontal walls. The enclosure exhibits a high aspect ratio $A = L/H$, where L and H denote its length along the –axis $\hat{x}$, and its height along the –axis $\hat{z}$, respectively. It is filled with a binary fluid characterized by a mass density ρ and dynamic viscosity μ.
The top and bottom horizontal walls are partially undulated, impermeable, and maintained at constant but different temperatures: $\hat{T}_b$ at the bottom and $\hat{T}_h$ at the top. The undulated segments extend over a dimensionless length L_w, and both vertical walls are perfectly thermally insulated.
The key control parameters of this system include the dimensionless length of the undulated section L_w, the dimensionless amplitude of the undulations a, and the Rayleigh number Ra.

The mathematical expressions describing the partial undulations of the horizontal walls (as shown in Fig. 1) are defined as follows.

On the lower wall

$$\text{for } \hat{z} = 0 \text{ and } \hat{x} \in \left[0, \hat{L}_w\right] \cup \left[\hat{L}_w + \hat{L}_c,\ L\right]:$$

$$\hat{z} = f_b\left(\hat{x}\right) = \pm \hat{a}\, sin\left(\frac{2\pi \hat{x}}{\hat{L}_w}\right). \tag{2}$$

On the upper wall

$$\text{For } \hat{z} = H \text{ and } \hat{x} \in \left[0, \hat{L}_w\right] \cup \left[\hat{L}_w + \hat{L}_c,\ L\right]:$$

$$\hat{z} = f_h\left(\hat{x}\right) = \pm\left[H + \hat{a}\, sin\left(\frac{2\pi \hat{x}}{\hat{L}_w}\right)\right]. \tag{3}$$

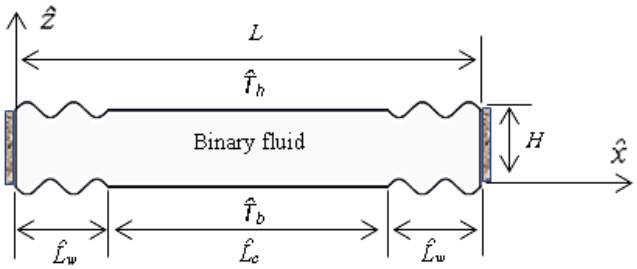

Fig. 1 Physical model of the problem

We propose, in a first step, to model the behavior of the fluid considered by adopting the following main assumptions:

- The fluid is Newtonian and incompressible, without chemical reaction, and viscous dissipation is negligible, which is suitable for liquid mixtures at low velocities generated by convection.
- The flow is laminar and two-dimensional, the latter being allowed by the fact that the third dimension is sufficiently large so that three-dimensional effects to be negligible.
- The Boussinesq approximation is used, considering density variations only in the buoyancy term, which

is valid for moderate thermal and concentration gradients and simplifies the resolution of the equations.
- Thermophysical properties are assumed constant, which is acceptable for limited temperature differences and facilitates numerical stability.
- Heat transfer follows Fourier's law and mass diffusion follows Fick's law including the Soret effect, while the Dufour effect (heat flux induced by a concentration gradient) is neglected due to its weak influence in dilute liquid mixtures [16].

2.2. Mathematical formulation

Based on these assumptions, the governing equations of the problem consist of a coupled system of partial differential equations that express the conservation of mass (Eq. 4), momentum (Eq. 5), energy (Eq. 6), and species concentration (Eq. 7). These equations, in their dimensional form, are written as follows [16]:

$$\nabla\vec{\hat{V}} = 0\,, \tag{4}$$

$$\rho_0\left(\frac{\partial\vec{\hat{V}}}{\partial\hat{t}}+\left(\vec{\hat{V}}\cdot\nabla\right)\vec{\hat{V}}\right)=\nabla\hat{P}+\mu\nabla^2\vec{\hat{V}}+$$
$$+\rho_0\left[1-\beta_T\left(\hat{T}-\hat{T}_0\right)-\beta_C\left(\hat{c}-\hat{c}_0\right)\right]\vec{g}\,, \tag{5}$$

$$\frac{\partial\hat{T}}{\partial\hat{t}}+\vec{\hat{V}}\nabla\hat{T}=\alpha\nabla^2\hat{T}\,, \tag{6}$$

$$\frac{\partial\hat{C}}{\partial\hat{t}}+\vec{\hat{V}}\nabla\hat{C}=D\nabla^2\hat{C}+D_T\hat{C}\left(1-\hat{c}\right)\nabla^2\hat{T}\,. \tag{7}$$

In this context, μ denotes the dynamic viscosity, α thermal diffusivity, D the mass diffusion coefficient, and D_T the thermodiffusion coefficient.

It is further assumed that in Eq. 7, the product $\hat{C}(1-\hat{c})$ remains nearly constant and can therefore be approximated by its value at the initial state $\hat{C}_0(1-\hat{c}_0)$.

According to the Boussinesq approximation, the density ρ in the buoyancy term, which is the driving force behind natural convection, is linearized:

$$\rho=\rho_0\left[1-\beta_T\left(\hat{T}-\hat{T}_0\right)-\beta_C\left(\hat{c}-\hat{c}_0\right)\right]. \tag{8}$$

In addition, the thermal and solutal expansion coefficients of the binary fluid mixture are defined as:

$$\beta_T=-\frac{1}{\rho_0}\left(\frac{\partial\rho}{\partial\hat{T}}\right)_{\hat{c}},\ \beta_c=-\frac{1}{\rho_0}\left(\frac{\partial\rho}{\partial\hat{c}}\right)_{\hat{T}}, \tag{9}$$

where $\hat{T}$ denotes the temperature and $\hat{c}$ the mass fraction of the heavier species, with (ρ_0, $\hat{T}_0$, and $\hat{c}_0$) being the corresponding reference values.

The corresponding boundary conditions for velocity, temperature, and species concentration are defined as follows:

- Hydrodynamic boundary conditions
  All the walls of the cavity are rigid, so:

$$\vec{\hat{V}}\left(\hat{x},\hat{z}=\left(0,H\right)\right)=\vec{\hat{V}}\left(\hat{x}=\left(0,L\right),\hat{z}\right)=\vec{0}\,. \tag{10}$$

- Thermal and mass boundary conditions
  Imposed temperatures on the horizontal walls:

$$\hat{T}\left(\hat{x},\hat{z}=f_b\left(\hat{x}\right)\right)=\hat{T}_b \text{ and } \hat{T}\left(\hat{x},\ \hat{z}=f_h\left(\hat{x}\right)\right)=\hat{T}_h,$$
$$\forall\,\hat{x}\in\left[0,L\right]. \tag{11}$$

The mass flux normal to the walls is zero:

$$\left(D\nabla\hat{C}+D_T\hat{C}_0\left(1-\hat{c}_0\right)\nabla\hat{T}\right)\vec{n}=\vec{0},\ \text{for}\ \hat{z}=f_b\left(\hat{x}\right)$$
$$\text{and}\ \hat{z}=f_h\left(\hat{x}\right),\forall\,\hat{x}\in\left[0,L\right]. \tag{12}$$

The heat and mass fluxes normal to the adiabatic and impermeable vertical walls are zero:

$$\frac{\partial\hat{T}}{\partial\hat{x}}=\frac{\partial\hat{C}}{\partial\hat{x}}=0\,,\ \text{for}\ \hat{x}=0\,,\ \hat{x}=L,\forall\,\hat{z}\in\left[0,H\right]. \tag{13}$$

2.3. Dimensionless conservation equations

To non-dimensionalize the governing Eqs. (4-7) and the boundary conditions Eqs. (10-13), the dimensionless variables defined in Table 1 are introduced.

Table 1

Dimensionless variables

Time	Coordinates	Velocities
$t=\dfrac{\hat{t}}{\hat{t}_{ref}}$	$(x,z)=\dfrac{(\hat{x}\,,\,\hat{z})}{H}$	$(U,V)=\dfrac{(\hat{U},\hat{V})}{\hat{V}_{ref}}$
Pressure	Temperature	Concentration
$P=\dfrac{\hat{P}}{\hat{P}_{ref}}$	$T=\dfrac{\hat{T}-\hat{T}_{ref}}{\hat{T}}$ $\hat{T}=\hat{T}_b-\hat{T}_h$	$C=\dfrac{\hat{C}-\hat{C}_{ref}}{\hat{C}}$ $\hat{C}=\hat{T}\hat{C}_0\left(1-\hat{c}_0\right)\dfrac{D_T}{D}$

The characteristic scales employed are:

$$\hat{t}_{ref}=\frac{H^2}{\alpha}\,,\ \hat{V}_{ref}=\frac{\alpha}{H}\,,\ \hat{P}_{ref}=\rho_0\frac{\alpha^2}{H^2}\,,\ \hat{T}_{ref}=\hat{T}_h\,,\ \hat{C}_{ref}=\hat{C}_0\,.$$

The problem is described by seven key dimensionless parameters:

- The thermal Rayleigh number $Ra=\dfrac{g\beta_T H^3\hat{T}}{\nu\alpha}$,
- The Prandtl number $Pr=\dfrac{\nu}{\alpha}$, where $\nu=\dfrac{\mu}{\rho_0}$,
- The Lewis number $Le=\alpha/D$,
- The separation ratio $\Psi=\dfrac{\beta_C}{\beta_T}\dfrac{D_T}{D}\hat{C}_0\left(1-\hat{c}_0\right)$,
- The shape factor $A=L/H$,
- The dimensionless length of the undulated section $L_w=\hat{L}_w/H$,
- The dimensionless undulation amplitude $a=\hat{a}/H$.

By substituting the dimensionless variables and parameters into Eqs. (4-7), the resulting system of dimensionless equations is derived:

$$\nabla \vec{V} = 0\,, \tag{14}$$

$$\frac{\partial \vec{V}}{\partial t} + \left(\vec{V}\cdot\nabla\right)\vec{V} = \nabla P + Pr\nabla^2\vec{V} + \\ + Ra\ Pr\left[T - \Psi C\right]\vec{e}_z\,, \tag{15}$$

$$\frac{\partial T}{\partial t} + \vec{V}\nabla T = \nabla^2 T\,, \tag{16}$$

$$\frac{\partial C}{\partial t} + \vec{V}\nabla C = \frac{1}{Le}\left(\nabla^2 C + \nabla^2 T\right), \tag{17}$$

The associated dimensionless boundary conditions are as follows.

- Hydrodynamic boundary conditions:

$$\vec{V}\left(x, z = (0,1)\right) = \vec{V}\left(x = (0, A), z\right) = \vec{0}\,, \tag{18}$$

- Thermal and mass boundary conditions:

$$T\left(x, z = f_b(x)\right) = T_b = 1, \\ T\left(x, z = f_h(x)\right) = T_h = 0, \text{ for } 0 \le x \le A, \tag{19}$$

$$\frac{\partial C}{\partial N}(x,z) + \frac{\partial T}{\partial N}(x,z) = 0, \\ \text{for } 0 \le x \le A,\ z = f_b(x) \text{ and } z = f_h(x), \tag{20}$$

where:

$$z = f_b(x) = \pm a\,sin\left(\frac{2\pi x}{L_w}\right), \\ \text{for } x \in \left[0, L_w\right] \cup \left[L_w + L_c, A\right], \tag{21}$$

$$z = f_h(x) = \pm\left[1 + a\,sin\left(\frac{2\pi x}{L_w}\right)\right], \\ \text{for } x \in \left[0, L_w\right] \cup \left[L_w + L_c, A\right], \tag{22}$$

$$\frac{\partial C}{\partial x}\left(x = (0, A), z\right) = \frac{\partial T}{\partial x}\left(x = (0, A), z\right) = 0, \\ \text{for } 0 \le z \le 1. \tag{23}$$

2.4. Lateral separation

To assess the efficiency of lateral species separation within the cavity, the dimensionless quantity S(z) is introduced, and defined as the difference between the local concentrations of the considered species on the left and right vertical walls:

$$S(z) = C_{pg}(z) - C_{pd}(z), \tag{24}$$

where C_{pg} and C_{pd} and denote the species concentrations along the left and right walls, respectively, at the same vertical position z. This metric quantifies the horizontal asymmetry of the concentration field, directly reflecting the separation effect induced by thermal gradients and convective-diffusive interactions within the binary fluid.

2.5. Heat transfer

The local heat transfer rate along the heated horizontal wall is quantified using the local Nusselt number, defined as:

$$Nu(\hat{x}) = -\left(\frac{\partial \hat{T}}{\partial n}\right)_{\hat{z}=f(\hat{x})} \frac{H}{\hat{T}}\,, \tag{25}$$

$$Nu(x) = -\left(\frac{\partial T}{\partial N}\right)_{z=f(x)}\,, \tag{26}$$

where the average of $Nu(x)$ along the heated horizontal wall is:

$$Nu_{moy} = \frac{1}{A}\int_0^A -\left(\frac{\partial T}{\partial N}\right)_{z=f(x)} dx\,. \tag{27}$$

3. Results and Discussion

This study addresses thermal convection within a rectangular cavity filled with a binary fluid (water–ethanol mixture), bounded by partially undulated horizontal isothermal walls, and subjected to thermal gradients imposed either from below or above. The dimensionless parameters governing the hydrodynamic, thermal, and mass transfer behavior of the system include the length of the undulated section L_w (1, 2, 3, 4), the undulation amplitude a (0, 0.05, 0.1), the thermal Rayleigh number Ra (-20, -100, 20, 100), the Lewis number Le = 100, a Prandtl number Pr = 10 corresponding to the water-ethanol binary mixture.

The dynamics of the flow and the distribution of concentration and temperature within the cavity are analyzed through streamlines, velocity fields, iso-concentration contours, and isotherms. The local and global heat transfer performance is assessed using the local and average Nusselt number.

The coupled system of partial differential equations governing natural convection and thermodiffusion: Eqs. (14-17), along with the corresponding boundary conditions: Eqs. (18-23), was solved numerically using the COMSOL Multiphysics software. The latter implements the Galerkin finite element method, ensuring the continuity of fluxes as well as the conservation of mass, momentum, energy, and chemical species.

The two-dimensional study domain was discretized, using a structured mesh composed of quadrilateral elements (140 × 40). However, a quadratic Lagrange interpolation was employed for the dependent variables.

The numerical calculations were conducted in transient regime starting from the initial condition at t = 0. The temporal evolution of the system was followed until a steady state was reached. The results discussed in this study correspond to this final steady-state configuration.

3.1. Model validation

Model accuracy is validated by comparison with the work of Ali Khouzam et al. (2013), concerning mass behavior of a binary fluid under mixed convection. The qualitative and quantitative agreement of concentration fields confirms the reliability of our simulation as it is illustrated

in Fig. 2.

3.2. Effect of the length of the undulated portion

3.2.1. Flow, mass, and thermal fields

In this section, the Rayleigh number is fixed at $Ra = 20$, corresponding to bottom heating, while the undulation amplitude is set to $a = 0.1$. Fig. 3 illustrates the influence of the variation of the length of the undulated section L_w (1, 2, 3, 4), on the hydrodynamic, thermal, and mass transport characteristics of the binary fluid within the cavity.

For $L_w = 1$, a dominant primary convective cell spans the cavity, exhibiting deformations near the left and right ends where the wall is undulated. This main cell encloses two secondary internal recirculations localized in the central flat region, along with two minor peripheral cells, one in the bottom right corner and the other in the top-left. The streamlines and velocity fields reveal a counterclockwise circulation in the primary and internal secondary cells, while the peripheral cells exhibit clockwise rotation. This flow structure, driven by both thermal and geometric effects, results in a mass distribution characterized by the migration of the fluid components toward the cavity extremities, with a maximum concentration $C_{max} = 2.08$ and velocity $V_{max} = 0.0074$.

As the undulated length increases to $L_w = 2$, the deformation of the main cell becomes more pronounced at both ends of the cavity. A new small internal cell forms in the added undulated region, rotating counterclockwise. The internal secondary cells in the flat region move closer together, intensifying the convective motion in that zone, though the flow is dampened in the undulated sections. This reorganization enhances species separation, with $C_{max} = 3.10$ where $V_{max} = 0.011$.

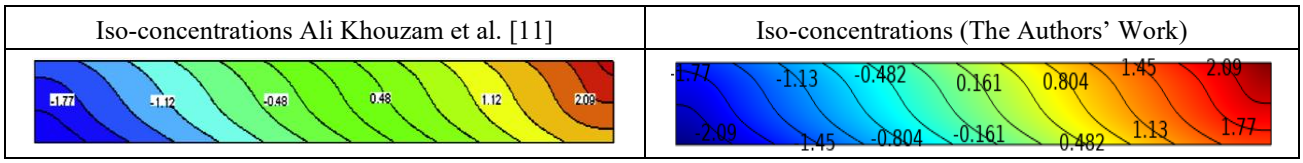

Fig. 2 Iso-concentrations for Rayleigh number $Ra = 53{,}75$ and Peclet number $Pe = 0{,}06$

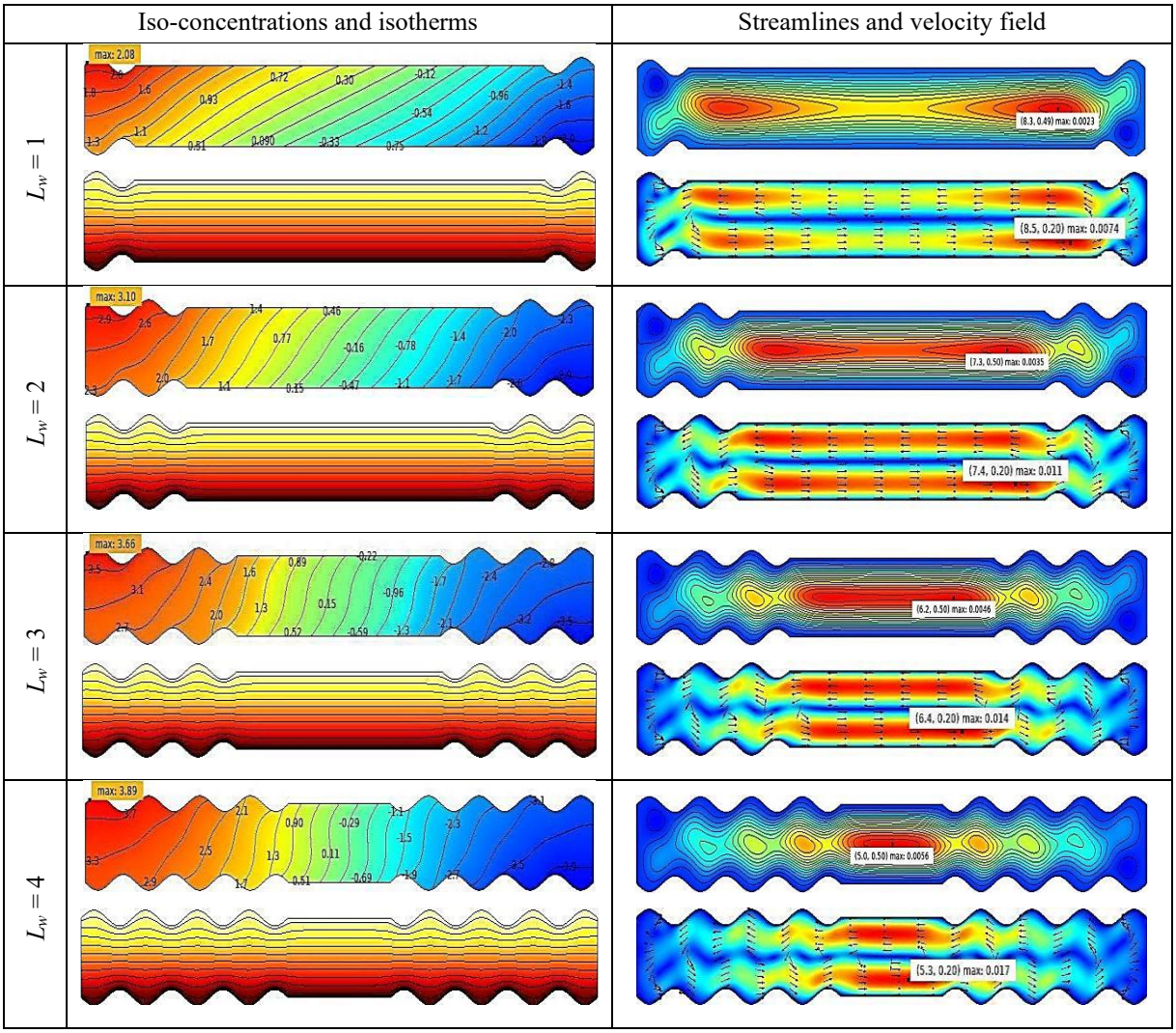

Fig. 3 Evolution of streamlines, velocity field, iso-concentrations, and isotherms for different values of the length L_w with $a = 0.1$, $Ra = 20$, $Le = 100$ and $\Psi = 0.1$

For $L_w = 3$, the undulated zone's influence further amplifies the main cell deformation and fosters the formation of another small counterclockwise cell in the newly added undulated segment. The two secondary cells in the central flat zone coalesce into a single structure with intensified counterclockwise flow, yielding a velocity peak of $V_{max} = 0.014$. The mass separation becomes more efficient, reaching $C_{max} = 3.66$.

At $L_w = 4$, the effects are further accentuated. The undulated ends support the development of additional internal cells with counterclockwise circulation, while a new central recirculation appears in the flat zone, also rotating counterclockwise. This configuration leads to enhanced flow intensity in the flat region, despite continued flow attenuation in the undulated zones. The mass separation reaches its highest observed value, $C_{max} = 3.89$ where $V_{max} = 0.017$, confirming the amplifying role of longer undulated sections.

The increase in L_w leads to an extension of the interaction zone between the wavy structures and the concentration field. This promotes the creation of more pronounced recirculation cells, which intensify the concentration gradients between the left and right walls.

Consequently, the lateral separation $S(z)$ of species is more effective as it is shown in Fig. 4.

The isotherms (Fig. 3) display localized distortions in the vicinity of the wavy boundaries, with an intensity that increases proportionally to the length of the undulated segment. The thermal field topology clearly indicates that heat transfer is predominantly governed by conduction rather than convection.

Fig. 5 illustrates the local Nusselt number along the heated wall. It increases towards the peaks and decreases towards the troughs. The maximum values occur at the ends of the wavy section where the vertical walls are adiabatic, while the minima appear at the transition between the wavy and flat areas. The effect of the length L_w of the wavy section is clearly visible, although the profile maintains symmetry.

Fig. 6 highlights the decrease in the average Nusselt number Nu_{-moy} as the length L_w of the wavy portion of the heated wall increases. This reduction is attributed to the growing number of flow damping zones within the troughs of the undulations.

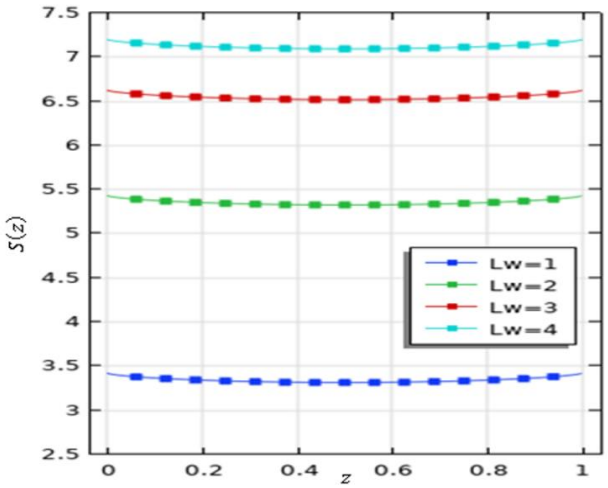

Fig.4 The lateral separation $S(z)$ for different values of the length L_w with $a = 0.1$, $Ra = 20$, $Le = 100$ and $\Psi = 0.1$

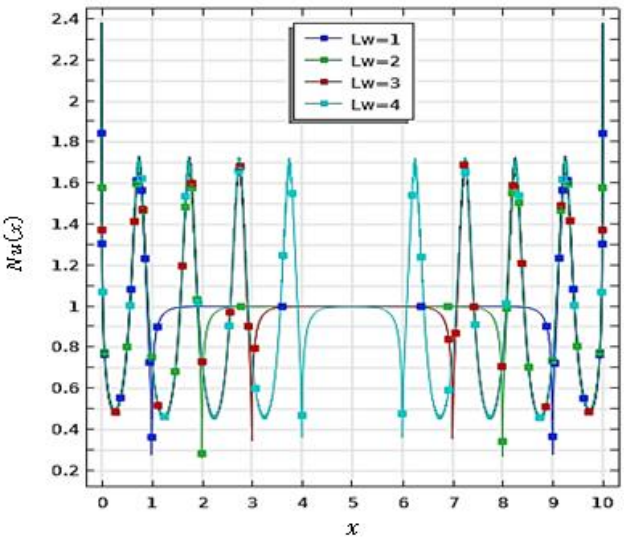

Fig. 5 The local Nusselt number Nu (x) for different values of the length L_w with $a = 0.1$, $Ra = 20$, $Le = 100$ and $\Psi = 0.1$

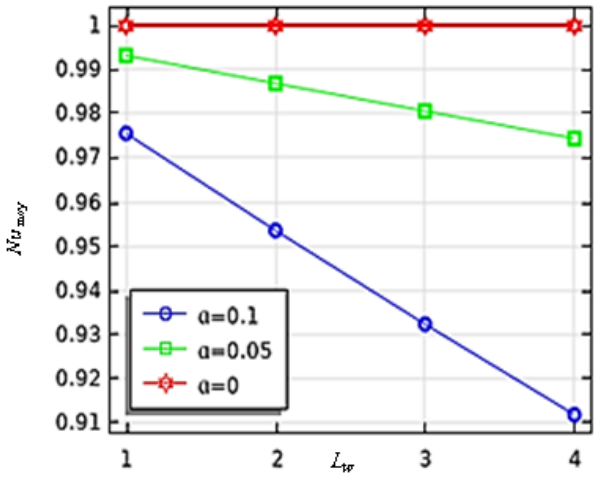

Fig. 6 The average Nusselt number Nu_{-moy} for different values of the length L_w. and different values of the amplitude a with $Ra = 20$, $Le = 100$ and $\Psi = 0.1$

3.3. Effect of the undulation amplitude

3.3.1 Flow, mass, and thermal fields

In this section, the Rayleigh number is fixed at $Ra = 20$, corresponding to heating from below, and the length of the undulated portion is set to $L_w = 4$. Fig. 7 presents the influence of the undulation amplitude a (0, 0.05, 0.1) on the hydrodynamic structure and the associated mass and thermal behavior of the binary fluid within the cavity.

For $a = 0$, i.e., in the absence of wall undulations, the flow exhibits a symmetric bicellular pattern, where the right vortex rotates counterclockwise and the left one clockwise. This symmetric flow configuration leads to a vertical mass stratification, as revealed by the iso-concentration lines, with the binary species migrating toward the horizontal walls. The maximum concentration observed is $C_{max} = 0.59$, and the peak velocity reaches $V_{max} = 0.0074$.

When the undulation amplitude increases to $a = 0.05$, the bicellular symmetry is disrupted. A dominant primary circulation cell emerges along the cavity, deformed

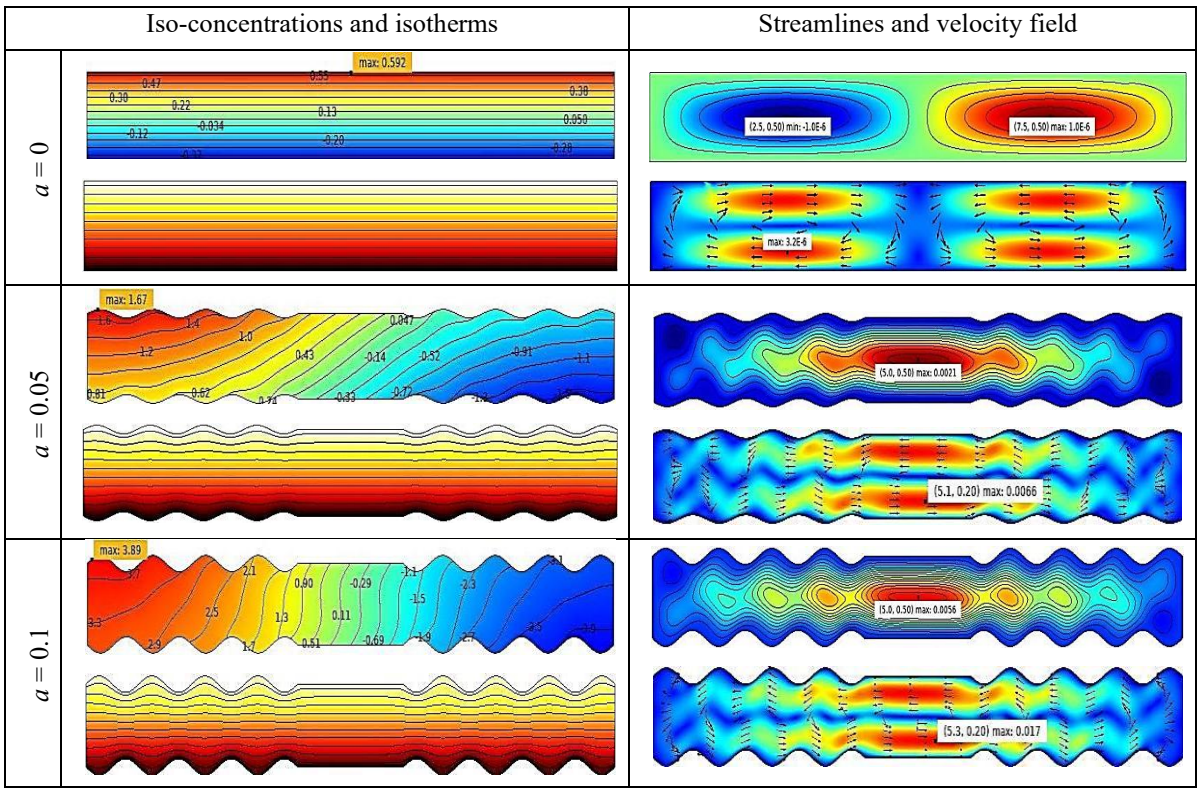

Fig. 7 Evolution of streamlines, velocity field, iso-concentrations, and isotherms for different values of the amplitude a with $L_w = 4$, $Ra = 20$, $Le = 100$ and $\Psi = 0.1$

at both ends within the undulated zones. Within the central flat region, an internal counterclockwise observed in the upper-left and lower-right corners, both exhibiting clockwise motion. This new flow structure promotes lateral separation of the fluid constituents toward the cavity's ends, resulting in a concentration peak of $C_{max} = 1.67$ and a slightly reduced flow velocity of $V_{max} = 0.0066$.

For to $a = 0.1$, the flow becomes increasingly complex. Additional small-scale vortices form within the main convective structure in the undulated regions, leading to enhanced flow intensity, with a maximum velocity of $V_{max} = 0.017$. This intensification drives a more effective separation of the fluid components toward the lateral boundaries, as indicated by a concentration peak of $C_{max} = 3.89$.

As shown in Fig. 8, the amplitude of the wall undulations acts as a catalyst for lateral species separation. Increasing the amplitude strengthens local velocity field disturbances, promoting a more significant transverse displacement of species toward the vertical walls.

As regards the thermal field (Fig. 7), the transition from flat to undulated walls induces localized undulations in the isotherms near the deformed boundaries. These distortions increase proportionally with the undulation amplitude. However, the overall structure of the isotherms remains largely preserved, indicating the predominance of thermal conduction over convection in the heat transfer mechanism within the cavity.

Fig. 9 reveals that the waviness amplitude significantly affects the local Nusselt number distribution. For $a = 0$, the distribution is uniform, while increasing a leads to pronounced spatial variations, with maxima at the edges and minima at the interface between wavy and flat areas.
Fig. 6 shows that increasing the amplitude a of the wall corrugation decreases the average Nusselt number due to enhanced flow attenuation in the wavy region, which weakens the convective heat transfer performance.

3.4. Effect of the Rayleigh number

3.4.1. Flow, mass, and thermal fields

In this section, the analysis is conducted for a fixed undulated portion length $L_w = 4$ and undulation amplitude $a = 0.1$. Fig. 10 illustrates the effect of varying the Rayleigh number Ra (–20, –100, 20, 100) on the hydrodynamic, mass, and thermal behavior of the binary fluid within the cavity.
Two thermal configurations are considered: heating from the top (Ra (–20, –100)) and heating from the bottom (Ra (20, 100)).

For $Ra = -20$, corresponding to heating from the top, the overall flow structure remains qualitatively similar to that observed for $Ra = 20$, but the direction of circulation is reversed due to the inversion of the buoyancy forces. The primary vortex and the internal secondary cells rotate clockwise, while the external corner cells rotate counterclockwise, as evidenced by the velocity field in Fig. 10. This flow configuration leads to a lateral separation of the fluid components, with a maximum concentration $C_{max} = 2.78$ and a velocity peak of $V_{max} = 0.011$.

When the Rayleigh number is decreased further to $Ra = -100$, the flow becomes more vigorous, with enhanced deformation of the main circulation cell and the emergence of additional secondary vortices in the bottom-left and top-right corners. The maximum velocity increases to $V_{max} = 0.028$, indicating a stronger convective motion. However, the separation of the fluid constituents is reduced compared to $Ra = -20$, as shown by a lower concentration peak

of $C_{max} = 1.63$. These effects are clearly illustrated in Fig. 10.

In the second thermal configuration, where the cavity is heated from below (Ra (20, 100)), the flow dynamics intensify, which can be observed on the vertical midline of the cavity through Fig. 10 and Fig. 11.

For $Ra = 20$, the velocity magnitude increases to $V_{max} = 0.017$, leading to a more pronounced segregation of number to $Ra = 100$, the flow becomes significantly more energetic, as indicated by the maximum velocity $V_{max} = 0.050$. The internal vortices in the undulated regions become more uniform in size and structure. Nonetheless, despite the increase in flow intensity, the species separation slightly diminishes compared to the case of $Ra = 20$, with a reduced

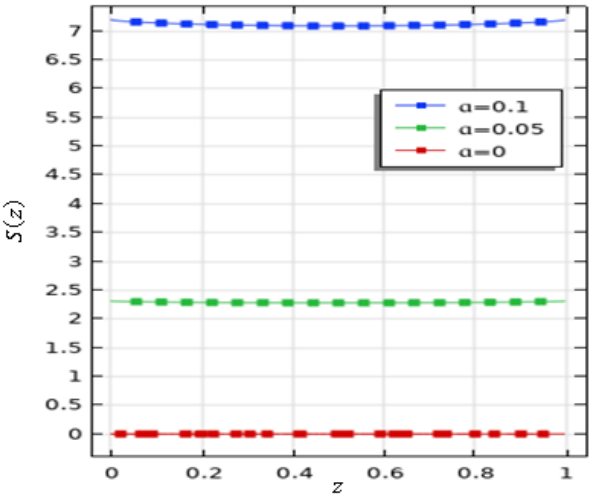

Fig. 8 The lateral separation $S(z)$ for different values of the amplitude a with $L_w = 4$, $Ra = 20$, $Le = 100$ and $\Psi = 0.1$

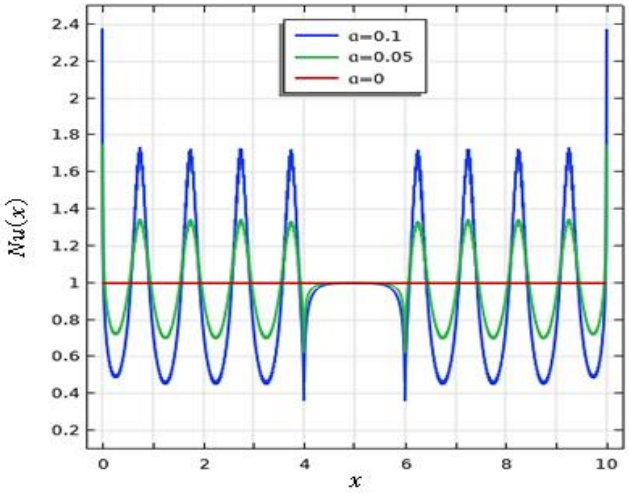

Fig. 9 The local Nusselt number $Nu(x)$ for different values of the amplitude a with $L_w = 4$, $Ra = 20$, $Le = 100$ and $\Psi = 0.1$

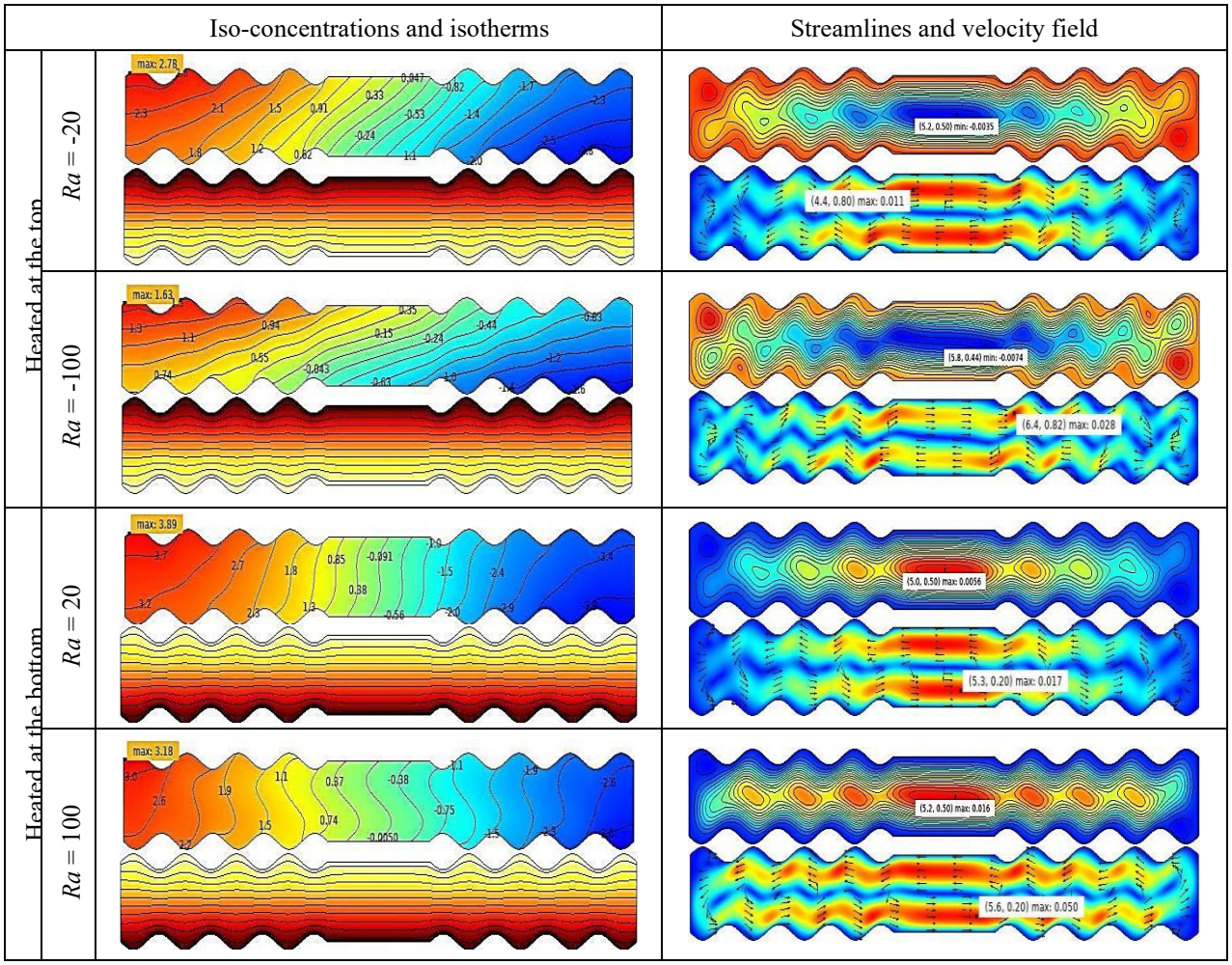

Fig. 10 Evolution of streamlines, velocity field, iso-concentrations, and isotherms for different values of the Rayleigh number Ra with $L_w = 4$, $a = 0.1$, $Le = 100$ and $\Psi = 0.1$

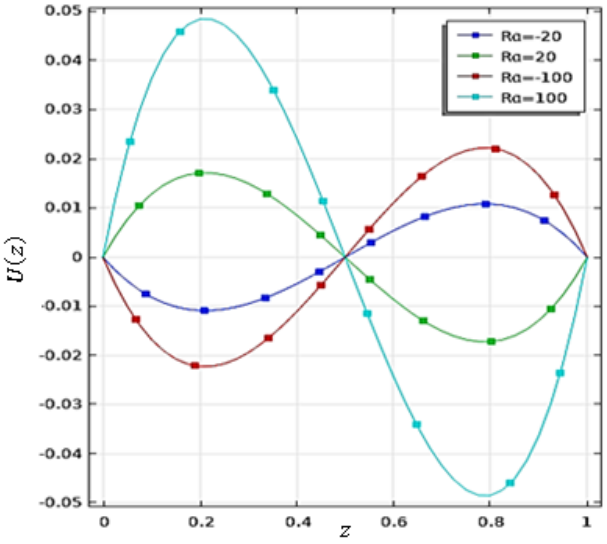

Fig. 11 The velocity $U(z)$ on the vertical midline for different values of the Rayleigh number Ra with $L_w = 4$, $a = 0.1$, $Le = 100$ and $\Psi = 0.1$

the binary species toward the lateral walls, with a peak concentration of $C_{max} = 3.89$. Upon increasing the Rayleigh concentration peak of $C_{max} = 3.18$. This reduction suggests that excessive flow intensification may disturb the optimal conditions for mass separation.

Fig. 12 clearly shows that heating from below ($Ra > 0$) promotes lateral separation better than heating from above ($Ra < 0$) and that the increase in the Ra number, which amplifies buoyancy forces, disrupts and decreases the lateral separation of species.

With respect to the thermal field, variations in the Rayleigh number over the considered range Ra (–20, –100, 20, 100) do not significantly affect the isotherm distribution shown in Fig. 10. The thermal gradient remains stable and uniform, with its orientation simply reversing based on the direction of heating (top or bottom). This behavior confirms that thermal conduction dominates over convection in this regime.

Fig. 13 illustrates the distribution of the local Nusselt number along the heated and partially undulated wall of length $L_w = 4$ and undulation amplitude $a = 0.1$, for

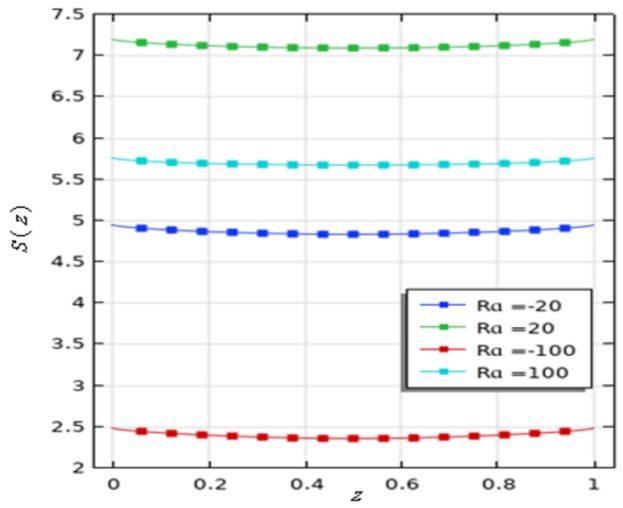

Fig. 12 The lateral separation $S(z)$ for different values of the Rayleigh number Ra with $L_w = 4$, $a = 0.1$, $Le = 100$ and $\Psi = 0.1$

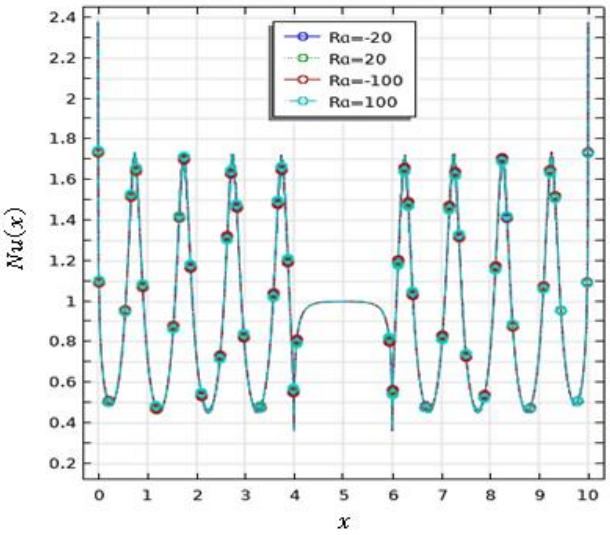

Fig. 13 The local Nusselt number $Nu(x)$ for different values of the Rayleigh number Ra with $L_w = 4$, $a = 0.1$, $Le = 100$ and $\Psi = 0.1$

various values of the Rayleigh number. The presence of the partial undulation significantly influences the spatial profile of the local Nusselt number, which retains a similar overall shape across the different Rayleigh numbers. The distribution exhibits symmetry with respect to the vertical midline, with peak values consistently observed at the left and right extremities of the heated wall, and a pronounced minimum at the interface between the undulated and flat sections.

4. Conclusion

In terms of numerical research, this current study has allowed the analysis of the influence of the partially wavy geometry of the horizontal walls in the presence of convection and thermodiffusion on the hydrodynamic, thermal, and mass behavior of a binary fluid confined in a modified rectangular cavity.

The qualitative analysis showed that the elongation of the wavy portion and the increase in the amplitude of the undulations profoundly modify the flow structure, promoting the formation of multiple recirculation cells and an intensification of the lateral transport of species. However, the temperature field remains dominated by conduction, while the concentration field reveals an increasingly marked lateral separation as the length and amplitude of the undulations increase, although the heat transfer performance, represented by the average Nusselt number, tends to decrease due to the local attenuation of convection in the hollow areas. Furthermore, it was observed that heating from below further promotes species separation than heating from above, while an excessive increase in the Rayleigh number leads to a disturbance of the separation regime.

In quantitative terms, the separation S increases significantly with the geometric parameters. In bottom heating, for a fixed amplitude $a = 0.1$, increasing the wavy length from $L_w = 1$ to $L_w = 4$ results in an approximately 112% increase in separation. Moreover, for $L_w = 4$, doubling the undulation amplitude from $a = 0.05$ to $a = 0.1$ leads to a 200% improvement. On the whole, these results confirm the decisive role of wavy geometry in intensifying the species separation phenomenon. Thus, this type of geometric configuration can be exploited in industrial separation systems,

where controlling mass transfer is a key factor for efficiency.

References

1. **De Groot, S. R.; Mazur, P**. 1962. Non-Equilibrium Thermodynamics, Amsterdam: North-Holland publishing company. 510p.
2. **Clusius, K.; Dickel, G**. 1938. Neues Verfahren zur Gasentmischung und Isotopentrennung (New Process for Separation of Gas Mixtures and Isotopes), Naturwissenschaften 26: 546. (in German) https://doi.org/10.1007/BF01675498.
3. **Furry, W. H.; Jones, R. C.; Onsager, L**. 1939. On the Theory of Iotope Separation by Thermal Diffusion, Physical Review 55(11): 1083. https://doi.org/10.1103/PhysRev.55.1083.
4. **De Groot, S. R.** 1942. Théorie Phénoménologique Du Procédé Thermo-Gravitationnel De Séparation Dans Un Liquide (Phenomenological Theory of the Thermo-Gravitational Process of Separation in a Liquid), Physica 9(8): 801-816. https://doi.org/10.1016/S0031-8914(42)80056-7.
5. **Lorenz, M.; Emery, A. H**. 1959. The packed thermal diffusion column, Chemical Engineering Science 11(1): 16-23. https://doi.org/10.1016/0009-2509(59)80069-5.
6. **Platten, J. K.; Bou-Ali, M. M.; Dutrieux, J. F**. 2003. Enhanced Molecular Separation in Inclined Thermogravitational Columns, The Journal of Physical Chemistry B 107(42):11-763. https://doi.org/10.1021/jp034780k.
7. **Elhajjar, B.; Mojtabi, A.; Marcoux, M.; Charrier-Mojtabi, M. C**. 2006. Study of thermogravitation in a horizontal fluid layer, Comptes Rendus Mecanique 334(10): 621-627. https://doi.org/10.1016/j.crme.2006.07.018.
8. **Charrier-Mojtabi, M. C; Elhajjar, B; Mojtabi, A.** 2007. Analytical and numerical stability analysis of Soret-driven convection in a horizontal porous layer, Physics of Fluids 19(12): 124104. https://doi.org/10.1063/1.2821460
9. **Elhajjar, B.; Mojtabi, A.; Charrier-Mojtabi, M. C.** 2009. Influence of vertical vibrations on the separation of a binary mixture in a horizontal porous layer heated from below, International Journal of Heat and Mass Transfer 52(1-2): 165-172. https://doi.org/10.1016/j.ijheatmasstransfer.2008.05.033
10. **Elhajjar, B.; Mojtabi, A.; Costeseque, P.; Charrier-Mojtabi, M. C.** 2010. Separation in an inclined porous thermogravitational cell, International Journal of Heat and Mass Transfer 53(21-22): 4844-4851. https://doi.org/10.1016/j.ijheatmasstransfer.2010.06.008.
11. **Khouzam, A.; Mojtabi, A.; Charrier-Mojtabi, M. C.; Ouattara, B**. 2013. Species separation of a binary mixture in the presence of mixed convection, International Journal of Thermal Sciences 73: 18-27. https://doi.org/10.1016/j.ijthermalsci.2013.05.012.
12. **Mojtabi, A.; Khouzam, A.; Yacine, L. A.; Charrier-Mojtabi, M. C.** 2019. Analytical and numerical study of Soret mixed convection in two sided lid-driven horizontal cavity: Optimal species separation, International Journal of Heat and Mass Transfer 139: 1037-1046. https://doi.org/10.1016/j.ijheatmasstransfer.2019.05.074.
13. **Mojtabi, A.; Sioud, K.; Bergeon, A.; Charrier-Mojtabi, M. C.** 2021. Numerical and Analytical Studies of Soret-Driven Convection Flow Inside an Annular Horizontal Porous Cavity, Fluids 6(10): 357. https://doi.org/10.3390/fluids6100357.
14. **Sioud, K.; Abdennadher, A.; Bergeon, A.; Kaddeche, S.; Charrier-Mojtabi, M. C.; Mojtabi, A.** 2022. Thermogravitational separation in porous vertical and horizontal cylindrical annular cells saturated by a binary mixture, The European Physical Journal E 45(5): 45. https://doi.org/10.1140/epje/s10189-022-00204-3.
15. **Mojtabi, A.; Sioud, K.; Charrier-Mojtabi, M. C.** 2025. Continuous Species Separation in an Open-Ended Porous Thermogravitational Column Using Mixed Convection, Transport in Porous Media 152: 52. https://doi.org/10.1007/s11242-025-02173-5.
16. **Platten, J. K.; Legros, J. C.** 1984. Convection in Liquids. Berlin: Springer-Verlag. 680p. https://link.springer.com/book/9783642820977.

M. A. Maazouzi, A. Benzegaou, N. Tarfaya

NUMERICAL SIMULATION OF A BINARY FLUID BEHAVIOR SUBJECTED TO THE COUPLING BETWEEN NATURAL CONVECTION AND THERMODIFFUSION IN A PARTIALLY WAVY CAVITY

S u m m a r y

The current numerical study aims to analyze the hydrodynamic, thermal, and mass transport behavior of a binary fluid under natural thermal convection and thermodiffusion within a modified horizontal rectangular cavity. The cavity is heated either from the bottom or the top, with isothermal, impermeable, and partially wavy horizontal walls. The simulation is based on the finite element method applied to the differential equations governing the coupling of natural convection and thermodiffusion. The results reveal that partial wall undulations significantly affect the binary fluid flow, leading to species migration toward the perfectly insulated vertical walls. The numerical analysis of the mass field of the studied fluid clearly indicates that the lateral species separation intensifies with bottom heating, increased undulated length, and greater wave amplitude. These geometrical parameters also significantly impact heat transfer, as characterized by the Nusselt number.

Keywords: convection, thermodiffusion, Soret effect, binary fluids, separation, undulated walls.

Received July 24, 2025
Accepted December 15, 2025